Available online at www.sciencedirect.com

ScienceDirect

journal homepage: www.elsevier.com/locate/he

# Plasmonic Bi nanoparticle decorated $BiVO_4$/rGO as an efficient photoanode for photoelectrochemical water splitting

*Palyam Subramanyam* [a], *Tanmoy Khan* [a], *Gudipati Neeraja Sinha* [a], *Duvvuri Suryakala* [b], *Challapalli Subrahmanyam* [a,*]

[a] *Department of Chemistry, Indian Institute of Technology Hyderabad, Kandi, 502285, Sangareddy, Telangana, India*
[b] *Department of Chemistry, GITAM University, Visakhapatnam, India*

## HIGHLIGHTS

- Synthesized BiNPs decorated $BiVO_4$/rGO photoanode for PEC water splitting.
- The chemical stability and plasmonic behavior of BiNPs improved by rGO surface.
- Bi–$BiVO_4$/rGO yielded current density of 6.05 mA/cm$^2$ with STH efficiency of 2.34%.
- High IPCE value of about 41% at 310 nm is achieved for the synthesized photoanode.

## GRAPHICAL ABSTRACT

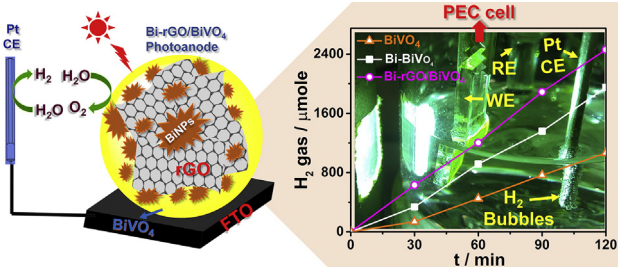


## ARTICLE INFO

*Article history:*
Received 9 June 2019
Received in revised form
8 August 2019
Accepted 21 August 2019
Available online 19 September 2019

*Keywords:*
Photoelectrochemical cell
Water splitting
Bismuth nanoparticles
Reduced graphene oxide
Surface plasmon resonance
Charge transportation

## ABSTRACT

We report the application of plasmonic Bi nanoparticles supported rGO/$BiVO_4$ anode for photoelectrochemical (PEC) water splitting. Nearly, 2.5 times higher activity was observed for Bi-rGO/$BiVO_4$ composite than pristine $BiVO_4$. Typical results indicated that Bi-rGO/$BiVO_4$ exhibits the highest current density of 6.05 mA/cm$^2$ at 1.23 V, whereas Bi–$BiVO_4$ showed the current density of only 3.56 mA/cm$^2$. This enhancement in PEC activity on introduction of Bi-rGO is due to the surface plasmonic behavior of BiNPs, which improves the absorption of radiation thereby reduces the charge recombination. Further, the composite electrode showed good solar to hydrogen conversion efficiency, appreciable incident photon-to-current efficiency and low charge transfer resistance. Hence, Bi-rGO/$BiVO_4$ provides an opportunity to realize PEC water splitting.



* *Corresponding author..*
E-mail address: csubbu@iith.ac.in (C. Subrahmanyam).
https://doi.org/10.1016/j.ijhydene.2019.08.214

## Introduction

Semiconductor based photoelectrochemical cells have been receiving great attention for water splitting due to their ability to absorb photons and generate voltage [1]. Alongside, the efficiency of photoelectrochemical (PEC) cells strongly depend on the generation of charge carriers, and their separation and mobility [2]. In order to display high PEC activity, the generation of charge carriers must be high and their recombination must be minimal [3]. The monoclinic-$BiVO_4$ is one such visible light active photoanodes for water oxidation whose bandgap lies between 2.4 and 2.5 eV, with suitably positioned valence band edge for oxygen evolution [4–6] and its superior chemical stability under light illumination [7]. Unfortunately, the reported conversion efficiencies are poor due to its low carrier mobility and fast recombination. To improve the mobility and minimize the recombination, $BiVO_4$ has been modified by various techniques such as formation of heterojunction with other semiconductors [8,9], metal doping [10,11], loading co-catalyst [12] etc. For example, in heterojunction systems like $TiO_2/BiVO_4$ [8] and $WO_3/BiVO_4$ [9] excellent PEC activity are reported. Metal doping such as Mo, W [10,11] is known to enhance the charge carrier concentration and electronic conductivity of $BiVO_4$. Furthermore, introduction of a co-catalyst on $BiVO_4$ also lead to significant improvement in PEC water oxidation due to its enhanced photostability [12].

Among the numerous modification methods, introduction of plasmonic metal nanoparticles gained sufficient attention owing to their ability to improve the visible-light absorption and prevent charge recombination due to the surface plasmon resonance (SPR) effect [13]. As a result, good photochemical energy conversion efficiency, photostability and interfacial charge transfer kinetics are observed [14]. Noble metals like Au [15,16] and Ag [14] have displayed surface plasmon resonance (SPR) property when combined with semiconductors [17]. For example, Jeong et al. fabricated $BiVO_4$ electrode decorated with Ag nanoparticles that showed ~3.3 times higher current than $BiVO_4$ film [18]. Kim et al. reported $Au/BiVO_4/ZnO$ heterojunction to obtain ~4.5 times higher photocurrent than pristine $BiVO_4$ photoelectrode [19]. Interestingly, bismuth nanoparticles (BiNPs) exhibit unique electronic properties such as SPR, high electron mean free path [20], high anisotropic fermi surface and small bandgap energy, etc [21,22]. Moreover, optical response of Bi nanostructures can be tuned between UV to IR region [23–26]. Toudert et al. reported that BiNPs exhibit tunable SPR phenomenon in near-UV to near-IR range region [27]. The heterojunction of Bi and $BiVO_4$ as reported by Wulan et al. shows two-fold increment in photocurrent density (1.96 mA/cm$^2$ at 1.23 V vs RHE) [28]. However, BiNPs have low chemical stability and poor SPR property. In order to showcase its SPR property, a support system is needed. With this background, we have used rGO as the support to improve charge transfer from BiNPs and thereby improving the overall PEC activity [14,29,30].

We fabricated Bi-rGO/$BiVO_4$ photoanode, where BiNPs were synthesized by chemical reduction method while rGO by Hummer's method. The fabrication of photoelectrodes was done by drop-casting. A systematic study was carried out to propose and understand the role of Bi-nanoparticles and rGO in improving the PEC performance of $BiVO_4$.

## Experimental section

### Materials

Bismuth acetate ($Bi(CH_3COO)_3$), bismuth nitrate trihydrate ($Bi(NO_3)_3\cdot 3H_2O$), acetic acid ($CH_3COOH$), sodium borohydride ($NaBH_4$), ethanol ($C_2H_5OH$), concentrated sulphuric acid ($H_2SO_4$), graphite powder, sodium nitrate ($NaNO_3$), potassium permanganate ($KMnO_4$), hydrogen peroxide ($H_2O_2$), acetylacetone, vanadyl acetylacetonate, hydrochloric acid (HCl). FTO glass used for fabrication of electrode has a sheet resistance of 13 Ω/cm$^2$ and is purchased from Aldrich. All the FTO glass plates are pre-cleaned with HCl solution (35%), followed by DI water and acetone.

### Synthesis of BiNPs

The synthesis of BiNPs was carried out by chemical reduction method. Briefly, ~193 mg of bismuth acetate was taken in 10 ml acetic acid, sonicated for 10 min to obtain a clear solution. To this solution, sodium borohydride was added dropwise under stirring. A brownish-black precipitate formed was washed with deionized water followed by ethanol via centrifugation. The obtained precipitate was dried at 60 °C.

### Fabrication of $BiVO_4$ and Bi–$BiVO_4$ photoanodes

Firstly, $BiVO_4$ photoanode was prepared by organic decomposition method followed by drop casting. The photoanode was fabricated as follows:173 mg of $Bi(NO_3)_3\cdot 5H_2O$ was dissolved in glacial acetic acid (0.4 ml) and sonicated to form a clear solution A. On the other hand, 95 mg of vanadyl acetylacetonate was taken in 4.6 ml of acetylacetone solution, sonicated for 5 min and labelled as solution B. Solution A was transferred to solution B and sonicated for 15 min, to obtain $BiVO_4$ solution. For fabrication of $BiVO_4$ photoanode, 0.5 ml of the as prepared solution was drop casted on FTO and annealed at 500 °C for 30 min. A yellow film of $BiVO_4$ was formed. Bi–$BiVO_4$ was fabricated by dissolving BiNPs in ethanol, sonication for 30 min, followed by drop-casting 0.5 ml onto $BiVO_4$ electrode and dried at 70 °C for 30 min.

### Synthesis of Bi-rGO and Bi-rGO/$BiVO_4$ photoanodes

GO and rGO were prepared by modified Hummer's method (provided in SI). The prepared BiNPs and GO are dissolved in ethanol and sonicated for 30 min. The resulting solution contains BiNPs decorated on the surface of rGO.

The Bi-rGO/$BiVO_4$ electrode was fabricated by drop-casting Bi-rGO (0.5 ml) solution on $BiVO_4$ electrode and dried at 70 °C for 30 min. The deposition scheme of Bi-rGO/$BiVO_4$ photoanode as presented in Scheme 1.

### Characterizations

Shimadzu UV-3600 instrument was used for collecting UV–Vis spectra for synthesized photoanodes, whereas the phase purity and presence of constituent materials was confirmed by powder X-ray diffraction (XRD) recorded by

using a PANalytical XpertPRO diffractometer. Surface morphologies of the samples were measured using a FESEM (Zeiss supra 40), whereas, TECNAI G-2 FEI (300 kV) was used to collect HR-TEM images.

### *Photoelectrochemical measurements*

Linear sweep voltammetric (I–V) studies were performed on LOT-Oriel with a 150 W Xe with a power density of ~100 mW $cm^{-2}$, which is measured by Newport Oriel instrument (Optical power/Energy meter-model 842.PE). Chronoamperometric (I-t) studies, electrochemical impedance spectroscopic (EIS) and cyclic voltammograms (CV) studies were performed on an Autolab PGSTAT 302 N using NOVA 2.1 software. Incident photon-to-current conversion efficiency (IPCE) data was performed by Oriel IQE-200 instrument with a 250 W quartz tungsten halogen lamp as a light source. A Trace-1310 GC equipped with a TCD was used to quantify hydrogen gas. The PEC measurements consist of a three electrode system, where the fabricated electrodes act as the working electrode (WE), Ag/AgCl, platinum (Pt) wire as the reference electrode (RE) and the counter electrode (CE) respectively. The fabricated electrodes were tested in 0.1 M $Na_2SO_4$ solution.

## Results and discussion

The formation of $BiVO_4$, BiNPs and GO was confirmed by XRD patterns as displayed in Fig. 1a. As noticed in Fig. 1a, $BiVO_4$ has monoclinic crystal lattice with (110), (121), (040), (200), (002), (112) and (051) crystal planes (JCPDS NO-140688) at 2θ values = 19.1, 28.91, 30.05, 34.79, 35.42, 40.07 and 42.6° respectively. BiNPs have rhombohedral crystal lattice with (003), (012), (104), (110), (015), (006), (202), (024), (116) and (122) planes (JCPDS NO-851331). For GO, a characteristic (002) plane of graphene oxide was confirmed from the peak at 2θ = 10.28° while, the Bi-rGO showed similar peaks as BiNPs, however, no rGO peak due to its low concentration (Fig. S1). Raman spectral analysis of synthesized samples BiNPs, Bi-rGO and Bi-rGO/$BiVO_4$ are displayed in Fig. 1b, which shows two characteristic vibrational bands at 68 and 96 $cm^{-1}$ corresponding to $E_g$ and $A_{1g}$ modes for BiNPs [31]. For Bi-rGO, the two additional peaks at 1338 and 1583 $cm^{-1}$ are due to the defect (D-band) and graphitic (G-band) of rGO respectively. This confirms that BiNPs are incorporated on the rGO sheets. Pure $BiVO_4$ and Bi–$BiVO_4$ showed similar Raman bands at 216, 375 and 825 $cm^{-1}$ which are due to asymmetric and symmetric bending vibrational bands and symmetric stretching vibration of $VO_4^{3-}$, respectively (Fig. S2). For Bi-rGO/$BiVO_4$ composite, extra peaks at 68, 1315 and 1553 $cm^{-1}$ are associated with the BiNPs, defect (D-band) and graphitic (G-band) bands of rGO respectively.

The absorption spectra of BiNPs, Bi-rGO, $BiVO_4$, Bi–$BiVO_4$ and Bi-rGO/$BiVO_4$ composites are shown in Fig. 2. The Bi nanoparticles displayed a sharp surface plasmon resonance peak centered at 320 nm that extended to near IR region. Further, BiNPs supported on rGO show improvement in the absorption intensity as shown in Fig. 2b, where absorption peaks are observed at 280 and 320 nm for rGO and SPR effect of BiNPs respectively. The absorption spectra of $BiVO_4$ reveal that they exhibit a narrow absorption with an absorption edge at 580 nm corresponding to the bandgap of 2.15 eV. BiNPs in combination with $BiVO_4$ lead to enhanced absorption. The absorption for Bi–$BiVO_4$ and Bi-rGO/$BiVO_4$ composites are shown in Fig. 2d.

The morphology of the samples was analyzed by FE-SEM and are displayed in Fig. 3. The synthesized Bi nanoparticles have a flower like morphology (Fig. 3a), whereas, rGO has a sheet like morphology (Fig. 3b). The surface morphologies of $BiVO_4$ appear to be porous with an average diameter of 300–350 nm as shown in Fig. 3c. Fig. 3d indicates the presence of BiNPs on $BiVO_4$. The composite Bi-rGO/$BiVO_4$ shows similar morphology like Bi–$BiVO_4$ and randomly aggregated with no specific shape but high surface roughness. The morphology of the composite is shown in Fig. 3e and the EDAX shown in Fig. 3f reveals the presence of BiNPs and the relative atomic percentages.

The HR-TEM images of BiNPs, Bi-rGO and Bi-rGO/$BiVO_4$ composite are shown in Fig. 4. The high resolution image of Bi-rGO and the composite are shown (Fig. 4b and d). The lattice spacing of 0.24 nm of BiNPs matches with the d-spacing calculated from (012) plane in XRD (JCPDS-851331) (Fig. 4a and c). Similarly, the lattice spacing of 0.31 nm matches with (121) plane for monoclinic $BiVO_4$ (JCPDS NO-140688) (Fig. 4e). SAED pattern of Bi-rGO/$BiVO_4$ composite is shown in Fig. 4f along with the planes.

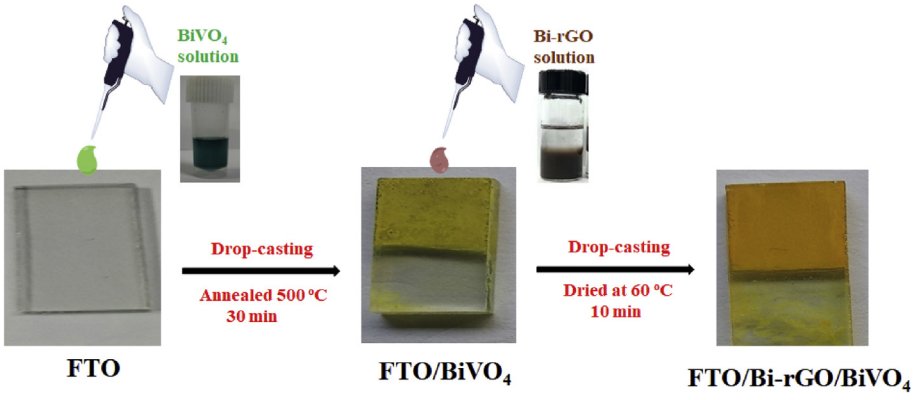


**Scheme 1 – The deposition scheme of Bi-rGO/$BiVO_4$ photoanode.**

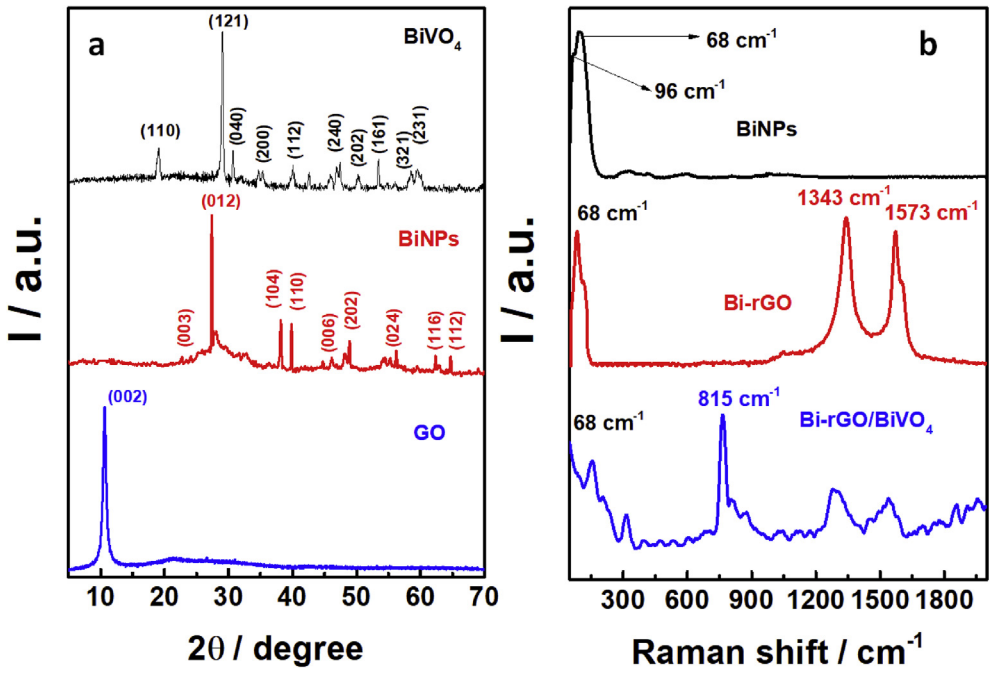


**Fig. 1 – (a) X-ray diffraction patterns of pristine $BiVO_4$, BiNPs and GO films (b) Raman spectra of BiNPs, Bi-rGO and Bi-rGO/$BiVO_4$ nanocomposite.**

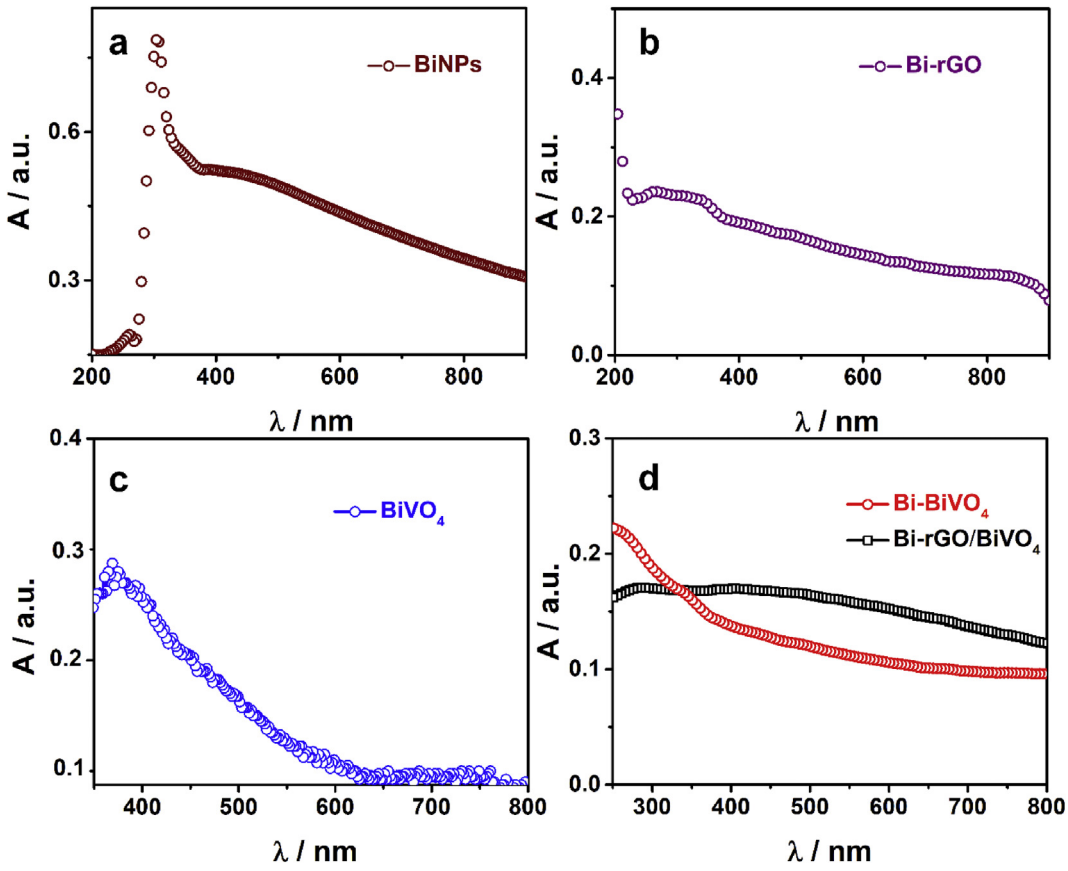


**Fig. 2 – Absorption spectra of (a) BiNPs (b) Bi-rGO (c) pristine $BiVO_4$ and (d) Bi–$BiVO_4$ and Bi-rGO/$BiVO_4$ nanocomposite.**

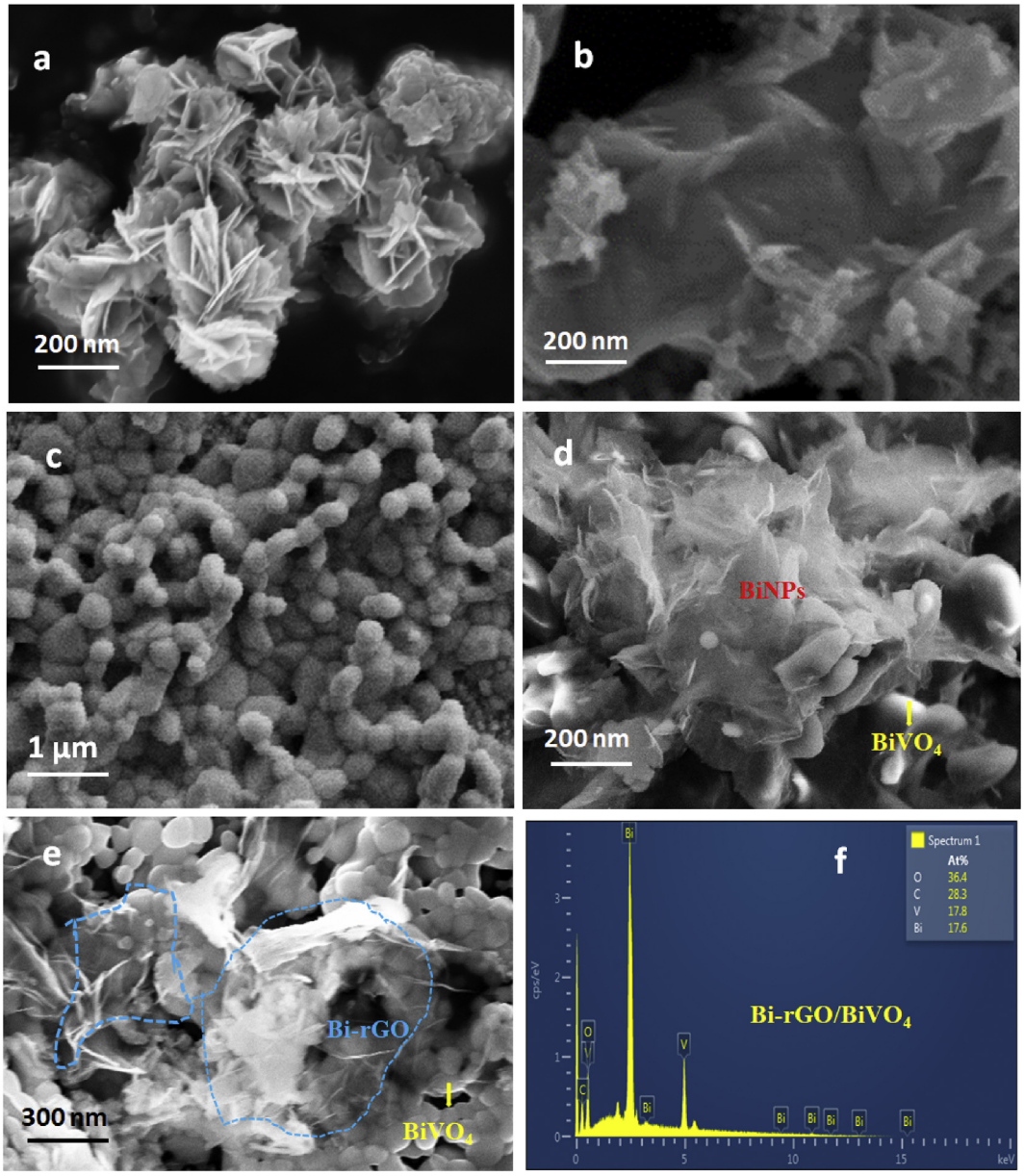


**Fig. 3 – FE-SEM images of (a) BiNPs (b) Bi-rGO (c) pristine $BiVO_4$ (d) Bi–$BiVO_4$ (e) Bi-rGO/$BiVO_4$ composite and (f) EDAX images of Bi-rGO/$BiVO_4$ composite.**

### *Photoelectrochemical studies*

The PEC studies were performed under visible light illumination. The LSV plots or current versus potential (I vs V) curves are displayed in Fig. 5a. The electrolyte used for the experiment is 0.1 M of $Na_2SO_4$. The potential was measured with respect to Ag/AgCl reference electrode and converted to RHE as shown in supporting information (SI). All the studied photoelectrodes show no photocurrent under dark conditions.

Upon light on and off mode (chopped illumination), the observed photocurrent density for $BiVO_4$, Bi–$BiVO_4$ and Bi-rGO/$BiVO_4$ nanocomposite is 2.39, 3.56 and 6.05 mA/cm$^2$ at 1.23 V, respectively. Bi-rGO/$BiVO_4$ composite produced the highest photocurrent density, which is two-times and nearly three-times higher than Bi–$BiVO_4$ and $BiVO_4$, respectively. The Bi-rGO/$BiVO_4$ has the onset potential of 0.15 V, which is lower than pristine $BiVO_4$ (0.26 V). The decrease in the onset potential for Bi-rGO/$BiVO_4$ can be due to increase in charge carrier separation and facile transfer due to incorporation of Bi and rGO. Among Bi–$BiVO_4$ and Bi-rGO/$BiVO_4$, the latter has higher photocurrent density due to conductive nature of rGO. Solar-to-hydrogen conversion (STH) for $BiVO_4$, Bi–$BiVO_4$ and Bi-rGO/$BiVO_4$ nanocomposite has been calculated by using equation (2) (SI), which are 0.82, 1.35 and 2.34% at 0.61 V respectively (Fig. 5b). This improved activity of Bi-rGO/$BiVO_4$ suggests that rGO stabilize BiNPs and improves the activity. The HER is shown in photograph (Fig. S3), which demonstrates

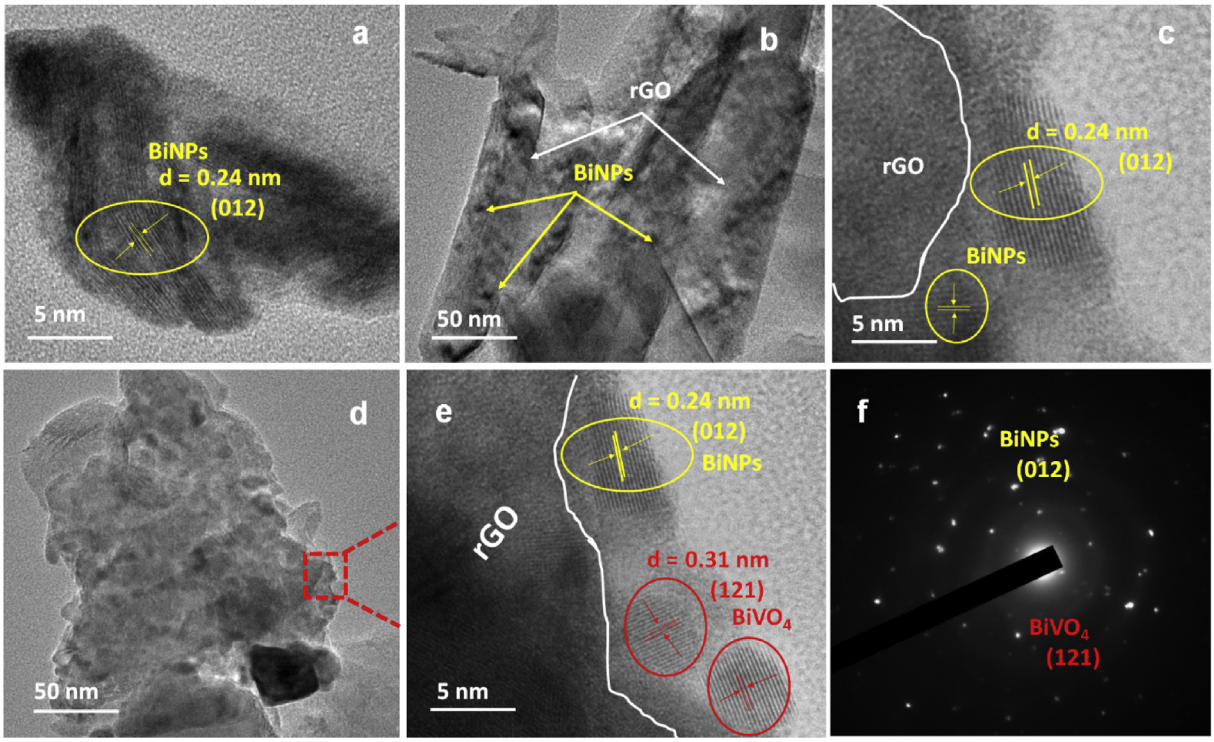


**Fig. 4 – HR-TEM images of (a) BiNPs, (b) and (c) are Bi-rGO, (d) and (e) are Bi-rGO/$BiVO_4$ composite, (f) SAED pattern of Bi-rGO/$BiVO_4$ composite.**

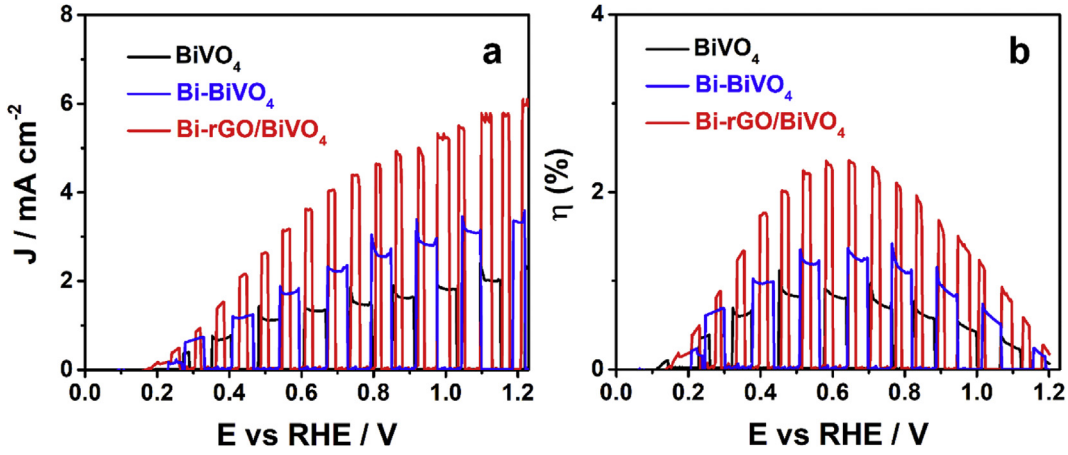


**Fig. 5 – (a) LSV plots and (b) STH efficiency of bare $BiVO_4$, Bi–$BiVO_4$ and Bi-rGO/$BiVO_4$ nanocomposite photoelectrodes under solar radiation.**

evolution of $H_2$ bubbles at the Pt CE during the PEC measurement.

The stability of the photoanodes is examined by chronoamperometric studies. The photocurrent for $BiVO_4$, Bi–$BiVO_4$ and Bi-rGO/$BiVO_4$ electrodes at 0.6 V vs RHE as a function of time is shown in Fig. 6a. It is worth mentioning that Bi-rGO/$BiVO_4$ nanocomposite exhibits long term stability up to 5000 s. The current density value obtained in LSV and chronoamperometry is consistent and in both studies, Bi-rGO/$BiVO_4$ composite showed higher current than pristine $BiVO_4$ and Bi–$BiVO_4$. The $H_2$ evolution, quantified by gas chromatography is plotted as a function of time. As shown in Fig. 6b, the Bi-rGO/$BiVO_4$ photoanode showed the maximum $H_2$ evolution of 2466 μmol at 2 h as compared to $BiVO_4$ (1071 μmol) and Bi–$BiVO_4$ (1941 μmol). Impressively, the composite exhibited nearly 2.5 times increment in $H_2$ evolution than pure $BiVO_4$ electrode. Thus, the quantification studies feature that Bi-rGO/$BiVO_4$ is a promising photoanode for PEC water splitting. The IPCE response of the all photoelectrodes is shown in Fig. 6c, Bi–$BiVO_4$ and Bi-rGO/$BiVO_4$ exhibit 34 and 41% conversion, respectively at 310 nm as compared to only 27% for pure $BiVO_4$. The IPCE expression is given in SI. The best performance is shown by Bi-rGO/$BiVO_4$ due to the formation of energetic hot electrons by plasmonic excitation of BiNPs. This

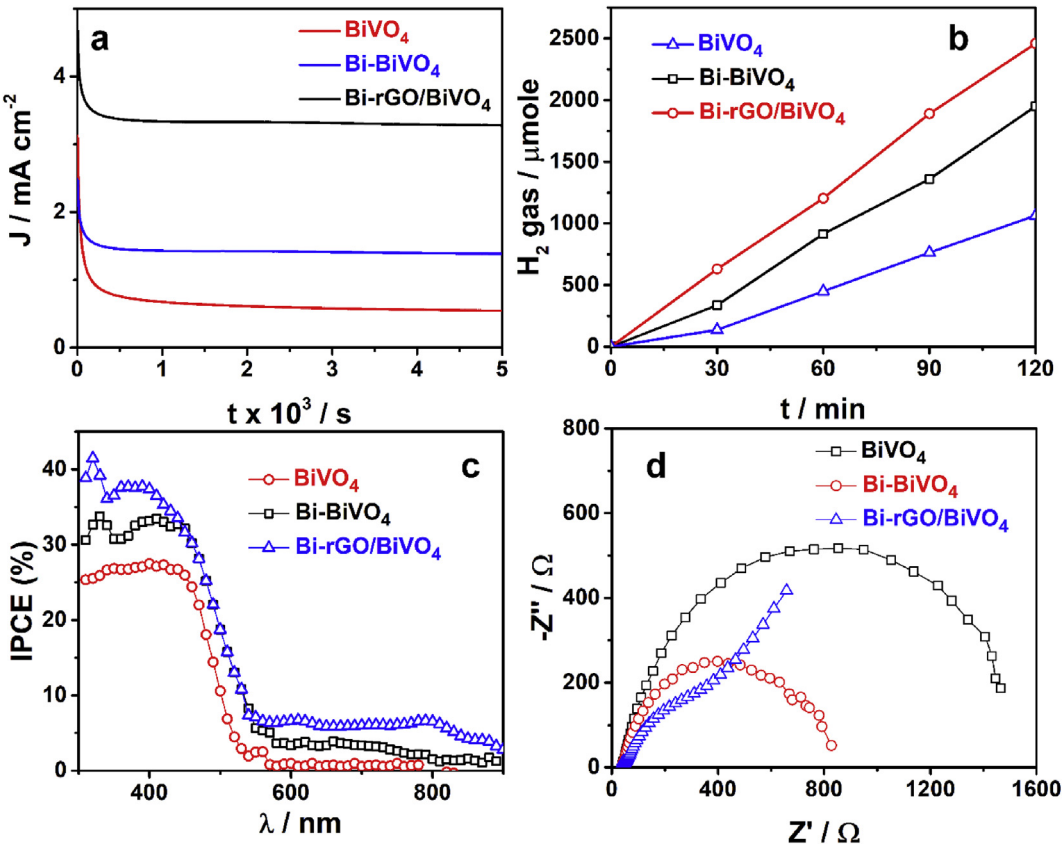


**Fig. 6 – (a) Stability of pure $BiVO_4$, Bi–$BiVO_4$ and Bi-rGO/$BiVO_4$ nanocomposite photoelectrodes at 1.23 V vs RHE during 5000 s. (b) $H_2$ evolution of Bi-rGO/$BiVO_4$ under light illumination under 2 h in comparison with pure $BiVO_4$ and Bi–$BiVO_4$. (c) IPCE of pristine $BiVO_4$, Bi–$BiVO_4$ and Bi-rGO/$BiVO_4$ photoelectrodes under monochromatic light radiation. (d) Nyquist plots for $BiVO_4$, Bi–$BiVO_4$ and Bi-rGO/$BiVO_4$ photoelectrodes.**

is also supported by the maximum photocurrent at around 310 nm. Impressively, the composite exhibited higher IPCE than other electrodes. This concludes that BiNPs on rGO suppresses the charge recombination and also facilitates higher charge injection transfer to the composite. BiNPs chemical stability and plasmon-induced hot electrons injection are complemented by the conductive nature of rGO. In addition, the high surface area and electrical conductivity of rGO improves the interfacial active sites in $BiVO_4$ which were unavailable in pure $BiVO_4$ thereby improving the dynamics of $BiVO_4$ for OER reaction.

In order to validate the ease of charge transfer at the electrode-electrolyte interface, EIS experiments were performed. The Nyquist plots obtained for $BiVO_4$, Bi–$BiVO_4$ and Bi-rGO/$BiVO_4$ photoanodes over the frequency range (1 kHz-1 Hz) under light irradiation are shown in Fig. 6d. All the electrodes have a solution resistance ~41 Ω. High $R_{ct}$ value of 1.46 kΩ for $BiVO_4$ is due to low charge separation and weak carrier mobility which are the main reasons for its poor water oxidation performance. However, BiNPs loading on the surface of $BiVO_4$ enhanced the charge carrier density since BiNPs acts as active sites for the PEC reaction which is evident from the $R_{ct}$ value of 0.80 kΩ as shown in Fig. 6d. Further, the rGO supported BiNPs on $BiVO_4$ significantly lower charge resistance ($R_{ct}$ value of 0.61 kΩ) which is attributed to the nature of rGO acting as a medium of transportation. In typical, the diameter of the semicircle represents charge transfer resistance ($R_{ct}$) in the Nyquist plot. Lower the $R_{ct}$, better the charge transfer process at the electrode-electrolyte interface [32–34]. Lowest $R_{ct}$ is observed for Bi-rGO/$BiVO_4$ composite over the fabricated photoanodes ($BiVO_4$ and Bi–$BiVO_4$). In simple terms, it could be explained as photogenerated electrons from $BiVO_4$ can be effectively collected with the help of Bi-rGO and consolidated electrons are transferred to counter electrode. Therefore, Bi-rGO/$BiVO_4$ exhibit dominated PEC response.

The mechanistic details of the electron transfer process in Bi-rGO/$BiVO_4$ composite photoelectrodes are shown in the schematic representation in Fig. 7c. The Fermi level of BiNPs, VB and CB positions of $BiVO_4$ are obtained from cyclic voltammetry (Fig. 7a and b). The procedure for calculation of band positions in the energy level diagram is presented in (SI). Due to absorption of solar radiation, excitons are generated. The surface plasmons are facilitated by BiNPs and electrons from Bi-rGO are injected into the CB of $BiVO_4$. Since, Bi-rGO facilitates quick charge injection, the generated charge carriers are efficiently transferred to FTO. Therefore, the presence of rGO accelerates the overall charge transport and hence better electron injection and enhanced PEC activity.

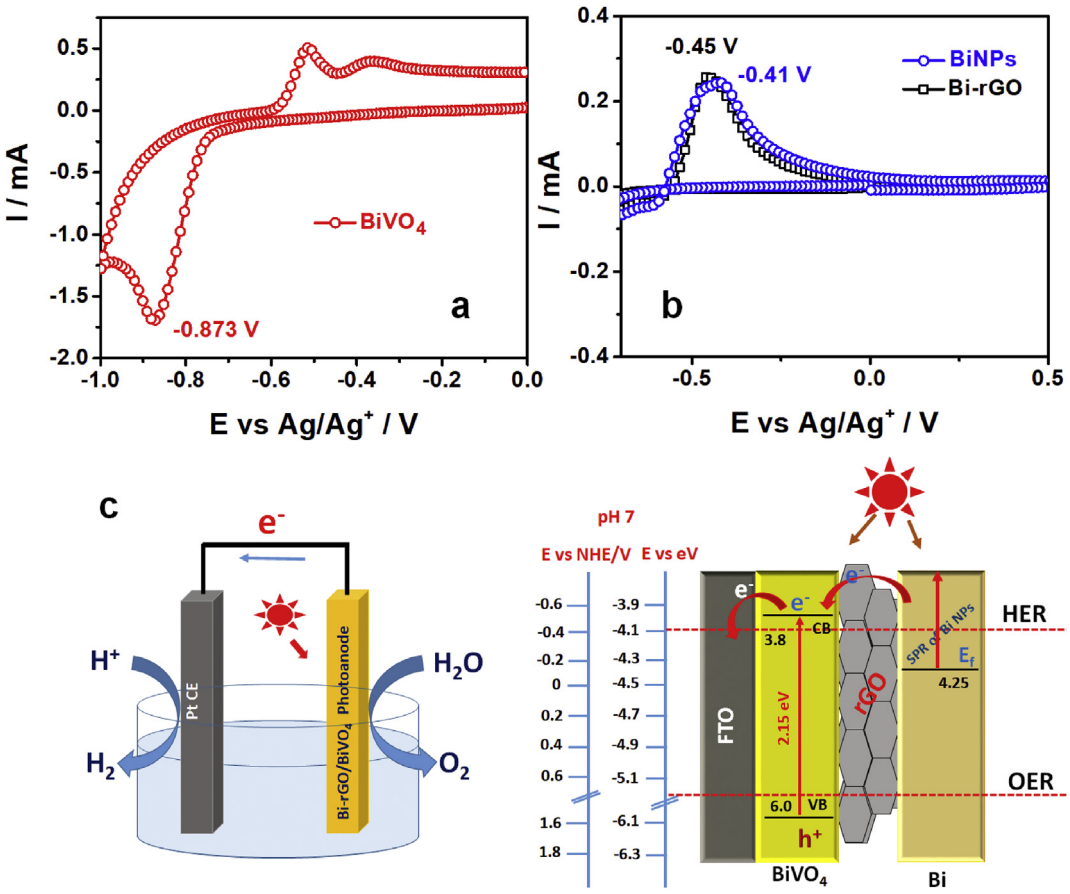


**Fig. 7 – CV plots of (a) bare $BiVO_4$ (b) BiNPs and Bi-rGO films (c) schematic diagrams of energy level alignment and charge transfer in Bi-rGO/$BiVO_4$ photoanode under solar light illumination.**

Briefly, the PEC activity could be explained by the light-driven holes in the VB of $BiVO_4$ that react with electrolyte to evolve oxygen and release protons. On the other side, the electrons are transferred through external circuit to counter electrode which favor HER. The whole movement of photogenerated carriers effectively takes place due to the conducting nature of Bi-rGO, which improves the charge transfer thereby improving the over all PEC performance for hydrogen production.

## Conclusions

A promising photoanode Bi-rGO/$BiVO_4$ was fabricated and used for photoelectrochemical water splitting reaction. This ternary photoanode displayed the best photocurrent density of 6.05 mA/$cm^2$ at 1.23 V over $BiVO_4$ and Bi–$BiVO_4$ with STH efficiency of 2.34% at 0.61 V. The best IPCE and less charge transfer resistance for Bi-rGO/$BiVO_4$ facilitates the charge separation and improves the charge carrier mobility. Chronoamperometric results revealed the stability of the photoanode over 5000 s. The SPR property of BiNPs is enhanced by rGO and efficient PEC activity of Bi-rGO/$BiVO_4$ is due to combined action of BiNPs in improving the charge carrier density and rGO in increasing the charge carrier mobility.

## Acknowledgements

PS thanks CSIR for a senior research fellowship. G.N.S thanks DST-Inspire (Reg No. IF170949), New Delhi, India for the award of research fellowship.

## Appendix A. Supplementary data

Supplementary data to this article can be found online at https://doi.org/10.1016/j.ijhydene.2019.08.214.

## REFERENCES

[1] Miller EL. Photoelectrochemical water splitting. Energy Environ Sci 2015;8:2809–10.
[2] Eftekhari A, Babu VJ, Ramakrishna S. Photoelectrode nanomaterials for photoelectrochemical water splitting. Int J Hydrogen Energy 2017;42:11078–109.
[3] Joy J, Mathew J, George SC. Nanomaterials for photoelectrochemical water splitting-review. Int J Hydrogen Energy 2018;43:4804–17.
[4] Tan HL, Amal R, Ng YH. Alternative strategies in improving the photocatalytic and photoelectrochemical activities of

visible light-driven $BiVO_4$: a review. J Mater Chem A 2017;5:16498–521.
[5] Tan HL, Amal R, Ng YH. Exploring the different roles of particle size in photoelectrochemical and photocatalytic water oxidation on $BiVO_4$. ACS Appl Mater Interfaces 2016;8:28607–14.
[6] Luo W, Yang Z, Li Z, Zhang J, Liu J, Zhao Z, Wang Z, Yan S, Yu T, Zou Z. Solar hydrogen generation from seawater with a modified $BiVO_4$ photoanode. Energy Environ Sci 2011;4:4046–51.
[7] Seabold JA, Choi KS. Efficient and stable photo-oxidation of water by a bismuth vanadate photoanode coupled with an iron oxyhydroxide oxygen evolution catalyst. J Am Chem Soc 2012 Jan 20;134(4):2186–92.
[8] Zhang H, Cheng C. Three-dimensional FTO/$TiO_2$/$BiVO_4$ composite inverse opals photoanode with excellent photoelectrochemical performance. ACS Energy Lett 2017;2:813–21.
[9] Chae SY, Lee CS, Jung H, Joo OS, Min BK, Kim JH, Hwang YJ. Insight into charge separation in $WO_3$/$BiVO_4$ heterojunction for solar water splitting. ACS Appl Mater Interfaces 2017;9:19780–90.
[10] Zhou M, Bao J, Xu Y, Zhang J, Xie J, Guan M, Wang C, Wen L, Lei Y, Xie Y. Photoelectrodes based upon Mo:$BiVO_4$ inverse opals for photoelectrochemical water splitting. ACS Nano 2014;8:7088–98.
[11] Subramanyam P, Vinodkumar T, Nepak D, Deepa M, Subrahmanyam C. Mo-doped $BiVO_4$@ reduced graphene oxide composite as an efficient photoanode for photoelectrochemical water splitting. Catal Today 2019;325:73–80.
[12] Ding C, Shi J, Wang D, Wang Z, Wang N, Liu G, Xiong F, Li C. Visible light driven overall water splitting using cocatalyst/$BiVO_4$ photoanode with minimized bias. Phys Chem Chem Phys 2013;15:4589–95.
[13] Srivastav A, Verma A, Khan SA, Smith YR, Satsangi VR, Shrivastav R, Dass S. Photoelectrochemical water splitting with 600 keV N2+ ion irradiated $BiVO_4$ and $BiVO_4$/Au photoanodes. Int J Hydrogen Energy 2019;44:13061–70.
[14] Patil SS, Mali MG, Hassan MA, Patil DR, Kolekar SS, Ryu SW. One-pot in situ hydrothermal growth of $BiVO_4$/Ag/rGO hybrid architectures for solar water splitting and environmental remediation. Sci Rep 2017;7:8404.
[15] Verma A, Srivastav A, Khan SA, Satsangi VR, Shrivastav R, Avasthi DK, Dass S. Enhanced photoelectrochemical response of plasmonic Au embedded $BiVO_4$/$Fe_2O_3$ heterojunction. Phys Chem Chem Phys 2017;19:15039–49.
[16] Wang Z, Wei Y, Wang X, Zhang W, Su J. Plasmonic Au nanopraticles modified nanopyramid-arrays $BiVO_4$ with enhanced photoelectrochemical activity. J Electrochem Soc 2019;166:H3138–45.
[17] Zhang L, Lin CY, Valev VK, Reisner E, Steiner U, Baumberg JJ. Plasmonic enhancement in $BiVO_4$ photonic crystals for efficient water splitting. Small 2014;10:3970–8.
[18] Jeong SY, Shin HM, Jo YR, Kim YJ, Kim S, Lee WJ, Lee GJ, Song J, Moon BJ, Seo S, An H. Plasmonic silver nanoparticle-impregnated nanocomposite $BiVO_4$ photoanode for plasmon-enhanced photocatalytic water splitting. J Phys Chem C 2018;122:7088–93.
[19] Kim S, Yu Y, Jeong SY, Lee MG, Jeong HW, Kwon YM, Baik JM, Park H, Jang HW, Lee S. Plasmonic gold nanoparticle-decorated $BiVO_4$/ZnO nanowire heterostructure photoanodes for efficient water oxidation. Catal Sci Technol 2018;8:3759–66.
[20] Dong F, Xiong T, Sun Y, Zhao Z, Zhou Y, Feng X, Wu Z. A semimetal bismuth element as a direct plasmonic photocatalyst. Chem Commun (J Chem Soc Sect D) 2014;50:10386–9.
[21] Li Y, Zhao Y, Wu G, Zhao J. Facile and efficient synthesis of bismuth nanowires for improved photocatalytic activity. Inorg Chem 2016;55:4897–905.
[22] Wang B, Feng W, Zhang L, Zhang Y, Huang X, Fang Z, Liu P. In situ construction of a novel Bi/CdS nanocomposite with enhanced visible light photocatalytic performance. Appl Catal, B 2017;206:510–9.
[23] Tian Y, Toudert J. Nanobismuth: fabrication, optical, and plasmonic properties-emerging applications. J Nanotechnol 2018;2018.
[24] Fan W, Li C, Bai H, Zhao Y, Luo B, Li Y, Ge Y, Shi W, Li H. An in situ photoelectroreduction approach to fabricate Bi/BiOCl heterostructure photocathodes: understanding the role of Bi metal for solar water splitting. J Mater Chem A 2017;5:4894–903.
[25] Wang J, Tang L, Zeng G, Liu Y, Zhou Y, Deng Y, Wang J, Peng B. Plasmonic Bi metal deposition and g-$C_3N_4$ coating on $Bi_2WO_6$ microspheres for efficient visible-light photocatalysis. ACS Sustainable Chem Eng 2016;5:1062–72.
[26] Wang Q, He J, Shi Y, Zhang S, Niu T, She H, Bi Y. Designing non-noble/semiconductor Bi/$BiVO_4$ photoelectrode for the enhanced photoelectrochemical performance. Chem Eng J 2017;326:411–8.
[27] Toudert J, Serna R, Jimenez de Castro M. Exploring the optical potential of nano-bismuth: tunable surface plasmon resonances in the near ultraviolet-to-near infrared range. J Phys Chem C 2012;116(38):20530–9.
[28] Wulan BR, Yi SS, Li SJ, Duan YX, Yan JM, Zhang XB, Jiang Q. Non-noble-metal bismuth nanoparticle-decorated bismuth vanadate nanoarray photoanode for efficient water splitting. Mater Chem Front 2018;2:1799–804.
[29] Yan L, Gu Z, Zheng X, Zhang C, Li X, Zhao L, Zhao Y. Elemental bismuth-graphene heterostructures for photocatalysis from ultraviolet to infrared light. ACS Catal 2017;7:7043–50.
[30] Du M, Xiong S, Wu T, Zhao D, Zhang Q, Fan Z, Zeng Y, Ji F, He Q, Xu X. Preparation of a microspherical silver-reduced graphene oxide-bismuth vanadate composite and evaluation of its photocatalytic activity. Materials 2016;9:160.
[31] Kumar B, Kaur G, Verma RK, Bahadur A, Rai SB. Bismuth functionalized PVA film: field, plasmonic and pH effect on PVA originated broad photoluminescence. RSC Adv 2016;6:26984–92.
[32] Wang T, Lv R, Zhang P, Li C, Gong J. Au nanoparticle sensitized ZnO nanopencil arrays for photoelectrochemical water splitting. Nanoscale 2015;7:77–81.
[33] Kang Q, Cao J, Zhang Y, Liu L, Xu H, Ye J. Reduced $TiO_2$ nanotube arrays for photoelectrochemical water splitting. J Mater Chem A 2013;1:5766–74.
[34] Su F, Wang T, Lv R, Zhang J, Zhang P, Lu J, Gong J. Dendritic Au/$TiO_2$ nanorod arrays for visible-light driven photoelectrochemical water splitting. Nanoscale 2013;5:9001–9.